


Bound states in the continuum in asymmetrical quantum-mechanical and electromagnetic waveguides

N. M. Shubin , A. V. Friman , V. V. Kapaev , and A. A. Gorbatshevich *

P.N. Lebedev Physical Institute of the Russian Academy of Sciences, 119991 Moscow, Russia

 (Received 25 June 2021; revised 24 August 2021; accepted 25 August 2021; published 7 September 2021)

We study transport properties and the formation of bound states in the continuum (BIC) in asymmetric quantum mechanical and electromagnetic waveguides. An analytical model for an arbitrary asymmetric two-terminal quantum mechanical waveguide is proposed, and conditions of BIC formation are formulated. We show that the Friedrich-Wintgen mechanism of BIC formation in a system coupled to two continua takes place regardless of the symmetry of the system as long as the proportionate coupling condition is fulfilled. This result is illustrated by numerical simulation of two-dimensional quantum billiard and optical waveguide with a cavity. Due to the universal wave nature of BIC, the proposed BIC formation mechanism allows one to obtain BICs in the broader class of quantum mechanical, electromagnetic, acoustic, and other types of structures.

DOI: [10.1103/PhysRevB.104.125414](https://doi.org/10.1103/PhysRevB.104.125414)

I. INTRODUCTION

Bound states in the continuum (BIC) take a prominent place among other interference phenomena in quantum mechanics and optics [1,2] because it took quite a long time to understand BIC origin's physical mechanisms, which combine peculiarities of both constructive and destructive interference of resonances. Initially considered as a purely mathematical trick invented by von Neumann and Wigner on the dawn of quantum mechanics [3], BIC is now recognized as a widespread physical phenomenon with many promising applications [4–12].

Original formulation of key properties and mechanism of BICs physics was performed within the quantum mechanical formalism [3,4] that provides more straightforward and transparent description compared to, e.g., optics. Theoretically, quantum mechanical BICs for electrons have been described in quantum conductors comprising electronic billiards (resonators) of various shapes [5,8,13], in multiply connected tight-binding quantum conductors [6,7,14], as well as in one-dimensional (1D) systems driven by an external oscillating field [15,16]. However, realization of electronic BICs might be questionable due to many-body interactions [16–19].¹ At the same time, technological control of structure parameters on a subwavelength scale needed for the experimental implementation of BIC is much easier to perform for electromagnetic [10,21–23] or acoustic waves [9,24] than for electrons. In particular, electromagnetic BICs have been successfully observed in experiments on electromagnetic

waveguides [25,26], photonic crystals [23,27,28], and metasurfaces [12,29,30].

In Ref. [1], classification of BICs has been presented, which comprises three main classes. These are symmetry-protected BICs (decoupling from continuum is due to different symmetries of the BIC and the continuum states wave functions) [31,32], Fabry-Perot BICs (the resonant state between two scatterers possessing perfect reflection at the BIC energy) [33], and Friedrich-Wintgen (FW) BICs [4]. All these mechanisms rely on universal properties of wave interference and are equally applicable to classical (electromagnetic, acoustic) or quantum (electrons) waves. In recent years a sophisticated FW mechanism attracted close attention [2] as a very productive approach for BIC design. In the FW model, BIC is formed in an open channel due to the destructive interference of waves scattered by two closed channels corresponding to localized states (when decoupled from an open channel). Though being initially developed for atomic physics, this model is very general and suitable for a large variety of wave phenomena [34–36]. In optics and acoustics, localized states inherent to FW mechanism can be constructed in resonators [9,37]. In quantum mechanics, an electronic analog of a classical resonator is, e.g., quantum billiard [5,8].

Being an infinitely long-living state, BIC can be related as a resonance with zero width, which corresponds to the scattering matrix pole at real axes. Hence, finding BIC in a specific model is equivalent to obtaining the null condition of the imaginary part of the scattering matrix pole [2]. A generic FW model is based on a common picture of wave interference without any explicit symmetry restrictions. However, in the case of arbitrary asymmetric waveguides (open channels) with continuous coordinate variables, finding poles of scattering matrix located on real axis is a multiparametric and cumbersome task (one should not only describe scattering on the localized state but simultaneously satisfy the resonance conditions for such state to exist) [11]. Until recently, BICs have been described explicitly mainly in symmetric waveguides

*gorbatsevichaa@lebedev.ru

¹Nevertheless, recently we have theoretically demonstrated the possibility of BICs formation in single-molecule conductors with Coulomb correlations taken into account (at least partially) within the *ab initio* calculations [20].

coupled to symmetric resonators (of different physical nature) [8,9], where symmetry conditions reduce the number of the independent system's parameters, which dramatically simplifies the task of searching for a BIC. Few exceptions include, for instance, BICs in 3D acoustic resonators [38], photonic crystal slabs [11], anisotropic media [39], and some other. However, the proposed structures either retain some symmetry elements [11,38] or are coupled to a single continuum [39], where the standard models are applicable.

To tackle the problem of BIC description in completely asymmetric structures, we take into consideration that the FW model [4] operates with a concept of localized states of fundamental origin (atomic states) rather than emergent localized states as in classical and quantum resonators. Hence one should expect that analysis of quantum interference in waveguides with localized states of fundamental origin (pre-existing localized states, e.g., in molecular conductors) will be more instructive and could provide some insight into how to gain the full power of the FW model and expand the range of system properties satisfying BIC condition to asymmetric systems. The fundamental difficulty of BIC description in asymmetric systems arises since, in general, geometrically different waveguides provide different continuous channels. Hence, according to the Pavlov-Verevkin theorem [40], one needs, e.g., three degenerate states to provide a BIC formation in a system coupled to two geometrically different waveguides. In this paper, we apply the recently developed theory of quantum transport in molecular conductors [14,41] to show that under specific analytical conditions, two continua of geometrically different waveguides can be effectively considered as single, which allows BIC formation in a quantum conductor possessing no symmetry elements for just two degenerate states. Within this theory, BIC can be considered either as resonance with zero width or as antiresonance with zero width. A separate description of exact positions of resonances and antiresonances makes it possible to establish simple BIC existence analytical rules in asymmetric waveguides. The derived relations are pretty universal and applicable to either quantum or electromagnetic waveguides comprising quantum billiards or optical resonators respectively. Analytic relations for BIC existence conditions are beneficial to determine a good initial approximation for more realistic numerical simulations.

The structure of our paper is as follows. In Sec. II the condition of proportionate coupling is deduced for BIC existence in a waveguide with asymmetric input and output. This condition is verified by numerical modeling of scattering problem for 2D quantum billiard in Sec. III. Also, we show here by 2D numerical modeling that proportionate coupling condition for BIC existence works for electromagnetic waveguides. A short conclusion is presented in Sec. IV.

II. THEORETICAL MODEL AND GENERAL RELATIONS

A. Model and transmission coefficient

We start the theoretical consideration with a general quantum-mechanical scattering problem, which can be applied to nuclear or atomic systems, molecular conductors, electronic waveguides, etc. To be specific, we focus on an electron resonator connected to two electron waveguides (we

will refer to them as left and right). We assume that each waveguide has only one propagating mode within the energy range of interest, i.e., we consider energies between the first and second states of transverse quantization. Hereinafter we neglect the interelectron Coulomb repulsion. Its influence on the BIC formation process deserves a special study and will be published elsewhere.

In the basis of eigenmodes, or equivalently in the basis of molecular orbitals (MO) in molecular electronics, the Hamiltonian of the resonator is diagonal:

$$\hat{H}_0 = \text{diag}(\varepsilon_1, \dots, \varepsilon_N). \quad (1)$$

Here ε_i is the energy of the i th state. Attaching the waveguide to this resonator results in the coupling of its eigenstates with the modes of the left and right waveguides. Assuming fully coherent transport, one can describe this coupling by the following matrices [42,43]

$$\hat{\Gamma}_{L,R}(E) = \mathbf{u}_{L,R}(E) \mathbf{u}_{L,R}^\dagger(E), \quad (2)$$

where vectors $\mathbf{u}_{L,R}$ are defined as:

$$\mathbf{u}_{L,R}(E) = \sqrt{\pi \rho_{L,R}(E)} (\gamma_1^{L,R}(E), \dots, \gamma_N^{L,R}(E))^\top. \quad (3)$$

with $\rho_{L,R}(E)$ being the density of modes per unit energy in the left or right waveguides and $\gamma_i^{L,R}(E)$ being the matrix element between the i th state of the resonator and the left or right waveguide mode with energy E .

Typically, the energy dependence of all $\gamma_i^{L,R}(E)$ is the same for any i (but different, in general, for the left and right waveguides) as it arises from the coupling to a mode with a particular energy [44]. Thus, energy and state index dependencies of $\gamma_i^{L,R}(E)$ can be factorized: $\gamma_i^{L,R}(E) = \gamma_i^{L,R} \gamma_{L,R}(E)$. Under this assumption, matrices $\hat{\Gamma}_{L,R}(E)$ and $\hat{\delta}_{L,R}(E)$ representing anti-Hermitian and Hermitian parts of the left or right waveguide self-energy, respectively, can be written as

$$\begin{aligned} \hat{\Gamma}_{L,R}(E) &= \mathbf{u}_{L,R} \mathbf{u}_{L,R}^\dagger g_{L,R}(E), \\ \hat{\delta}_{L,R}(E) &= \mathbf{u}_{L,R} \mathbf{u}_{L,R}^\dagger h_{L,R}(E). \end{aligned} \quad (4)$$

Here $g_{L,R}(E) = \pi \rho_{L,R}(E) |\gamma_{L,R}(E)|^2$, $h_{L,R}(E)$ is a Hilbert transform of $g_{L,R}(E)$, and coupling vectors $\mathbf{u}_{L,R}$ are energy independent:

$$\mathbf{u}_{L,R} = (\gamma_1^{L,R}, \dots, \gamma_N^{L,R})^\top. \quad (5)$$

Transmission coefficient can be calculated by the standard Landauer-Büttiker-Fisher-Lee formula [45]:

$$T(E) = \text{Tr}[\hat{\Gamma}_L(E) \hat{G}^r(E) \hat{\Gamma}_R(E) \hat{G}^a(E)]. \quad (6)$$

Here $\hat{G}^r(E) = [\hat{G}^a(E)]^\dagger = [E\hat{I} - \hat{H}_{\text{eff}}(E)]^{-1}$ is the retarded or advanced Green's function with

$$\hat{H}_{\text{eff}}(E) = \hat{H}_0 + \hat{\delta}_L(E) + \hat{\delta}_R(E) - i\hat{\Gamma}_L(E) - i\hat{\Gamma}_R(E) \quad (7)$$

being the Feshbach's effective Hamiltonian [46]. Using factorization (4) and applying Sherman-Morrison theorem [47] and matrix determinant lemma [48] to Eq. (6), one can arrive to the following expression for the transmission coefficient:

$$T(E) = \frac{|P(E)|^2}{|P(E)|^2 + |Q(E)|^2}, \quad (8)$$

with

$$P(E) = 2\sqrt{g_L(E)g_R(E)}F_{LR}(E), \quad (9)$$

$$Q(E) = \{1 - F_{LL}(E)[h_L(E) + ig_L(E)]\}\{1 - F_{RR}(E)[h_R(E) - ig_R(E)]\} - |F_{LR}(E)|^2[h_L(E) + ig_L(E)][h_R(E) - ig_R(E)], \quad (10)$$

where

$$F_{LL}(E) = \mathbf{u}_L^\dagger (E\hat{I} - \hat{H}_0)^{-1} \mathbf{u}_L = \sum_{i=1}^N \frac{|\gamma_i^L|^2}{E - \varepsilon_i},$$

$$F_{RR}(E) = \mathbf{u}_R^\dagger (E\hat{I} - \hat{H}_0)^{-1} \mathbf{u}_R = \sum_{i=1}^N \frac{|\gamma_i^R|^2}{E - \varepsilon_i},$$

$$F_{LR}(E) = \mathbf{u}_L^\dagger (E\hat{I} - \hat{H}_0)^{-1} \mathbf{u}_R = \sum_{i=1}^N \frac{\gamma_i^{L*} \gamma_i^R}{E - \varepsilon_i}. \quad (11)$$

Formula (8) for the transmission coefficient is typical for any two-terminal quantum conductor and allows for an illustrative analysis of main interference features: a real root of function $P(E)$ corresponding to a zero antiresonance and a real root of function $Q(E)$ describing a unity-valued resonance [14].

It is important to note that here Eq. (8) with $P(E)$ and $Q(E)$ functions (9) and (10) are derived in the basis of eigenstates (MO basis in molecular electronics) contrary to Ref. [14], where it was performed in the tight-binding (atomic orbital) basis. Eigenstates (MO) approach is more appropriate for the treatment of systems with continuous coordinate variables such as quantum mechanical and optical waveguides with cavities discussed in the numerical simulation section below.

Functions $P(E)$ and $Q(E)$ as they are defined in Eqs. (9) and (10) are rational functions of energy. However, as one can see from the transmission coefficient (8) that they are defined up to a common factor, and hence one can multiply them by $\det(E\hat{I} - \hat{H}_0)$ to make holomorphic in convenience with the definition in Ref. [14].

B. Bound states in the continuum and proportionate coupling condition

Transmission coefficient formula (8) provides a natural condition for a bound state in the continuum (BIC) to arise. Indeed, the presence of a common real root of $P(E)$ and $Q(E)$ functions indicates the presence of a real eigenvalue of the effective Feshbach's Hamiltonian [14], which means the formation of a BIC [1]. If all the transmission resonances are well separated and narrow (couplings to the waveguides are much smaller than quantum system energy level spacing: $|\gamma_i^{L,R}|^2 \ll \min|\varepsilon_i - \varepsilon_j|$ for any i and $j \neq i$), then a BIC can form from the i th eigenstate for $\gamma_i^L = \gamma_i^R = 0$. In particular, this is the case of a symmetry-protected BIC.

According to the FW mechanism [4], a more complicated picture takes place when two states have close energies at certain values of the parameters. Without loss of generality, we suppose, there are two eigenstates $|1\rangle$ and $|2\rangle$ with

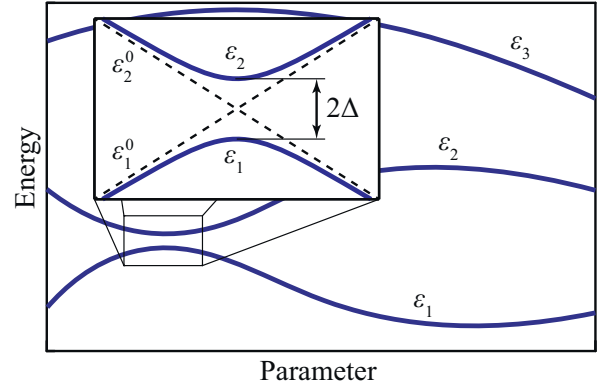


FIG. 1. Schematic dependence of the eigenstates energy on some parameter. The avoided crossing region is magnified and reparametrization by eigenvalues of $\hat{H}_{2 \times 2}$ from Eq. (12) is illustrated. Blue thick solid lines describe exact eigenvalues $\varepsilon_{1,2}$ in the avoided crossing region, and thin black dashed lines show their asymptotics $\varepsilon_{1,2}^0$.

energies ε_1 and ε_2 such that $|\varepsilon_1 - \varepsilon_2| \ll |\varepsilon_1 - \varepsilon_i|, |\varepsilon_2 - \varepsilon_i|$ for any $i \neq 1, 2$. Assume, functions $g_{L,R}(E)$ and $h_{L,R}(E)$ are smooth in the vicinity of $\varepsilon_{1,2}$ and can be treated as constants: $g_{L,R}(E) \approx g_{L,R}[1/2(\varepsilon_1 + \varepsilon_2)] = g_{L,R} = \text{const} > 0$ and $h_{L,R}(E) \approx h_{L,R}[1/2(\varepsilon_1 + \varepsilon_2)] = h_{L,R} = \text{const}$.

In general, in an arbitrary nonsymmetric quantum system, eigenvalues demonstrate avoided crossing behavior rather than crossing with degeneracy [8,49]. In order to take this into account explicitly, one can approximate close energies $\varepsilon_{1,2}$ as eigenvalues of some effective two-level model with the Hamiltonian

$$\hat{H}_{2 \times 2} = \begin{pmatrix} \varepsilon_1^0 & \Delta \\ \Delta & \varepsilon_2^0 \end{pmatrix} \quad (12)$$

given by the following relations:

$$\varepsilon_{1,2} = \frac{\varepsilon_1^0 + \varepsilon_2^0}{2} \pm \sqrt{\Delta^2 + \frac{(\varepsilon_1^0 - \varepsilon_2^0)^2}{4}}. \quad (13)$$

In Eqs. (12) and (13), $\varepsilon_{1,2}^0$ describes the asymptotic of $\varepsilon_{1,2}$ away from the avoided crossing region² and $2\Delta > 0$ defines the minimal split between them (see Fig. 1). In this case, $\gamma_{1,2}^{L,R}$ are matrix elements away from the avoided crossing region.

Using the introduced above two-level reparametrization in the vicinity of $\varepsilon_{1,2}$, one can get numerators of $P(E)$ and $Q(E)$ functions as square polynomials in E space (see Appendix A). The condition for $P(E)$ and $Q(E)$ to have a common real root, i.e., the condition for BIC formation, can be derived from

²The avoided crossing region in the parameter space is identified as $|\varepsilon_1^0 - \varepsilon_2^0| \lesssim \Delta$.

analysis of the resultant of their numerators:

$$\begin{aligned} & \text{Res}\{P(E)[(E - \varepsilon_1^0)(E - \varepsilon_2^0) - \Delta^2], Q(E)[(E - \varepsilon_1^0)(E - \varepsilon_2^0) - \Delta^2]\} \\ &= 4g_L g_R \left\{ \left[\varepsilon_2^0 - \varepsilon_1^0 + \Delta \left(\frac{\gamma_1^L}{\gamma_2^L} - \frac{\gamma_2^L}{\gamma_1^L} \right) \right] C_1 + \left(\frac{\gamma_1^R}{\gamma_1^L} - \frac{\gamma_2^R}{\gamma_2^L} \right) C_2 \right\} \left\{ \left[\varepsilon_2^0 - \varepsilon_1^0 + \Delta \left(\frac{\gamma_1^R}{\gamma_2^R} - \frac{\gamma_2^R}{\gamma_1^R} \right) \right] C_3 + \left(\frac{\gamma_2^L}{\gamma_2^R} - \frac{\gamma_1^L}{\gamma_1^R} \right) C_4 \right\}, \quad (14) \end{aligned}$$

where C_i are some complex quantities. Resultant (14) turns to zero if either of the two expressions in the braces vanishes. In general, a linear combination of two complex numbers C_1 and C_2 (or, equivalently, C_3 and C_4) with real coefficients can turn to zero only if both real coefficients turn to zero simultaneously. Thus, generally, functions $P(E)$ and $Q(E)$ have a common real root at energy

$$\begin{aligned} E = E_{\text{BIC}} &= \frac{\varepsilon_1^0 + \varepsilon_2^0}{2} - \frac{\Delta}{2} \left(\frac{\gamma_1^L}{\gamma_2^L} + \frac{\gamma_2^L}{\gamma_1^L} \right) \\ &= \frac{\varepsilon_1^0 + \varepsilon_2^0}{2} - \frac{\Delta}{2} \left(\frac{\gamma_1^R}{\gamma_2^R} + \frac{\gamma_2^R}{\gamma_1^R} \right) \end{aligned} \quad (15)$$

if the following conditions are fulfilled:

$$\varepsilon_2^0 - \varepsilon_1^0 = \Delta \left(\frac{\gamma_2^L}{\gamma_1^L} - \frac{\gamma_1^L}{\gamma_2^L} \right) = \Delta \left(\frac{\gamma_2^R}{\gamma_1^R} - \frac{\gamma_1^R}{\gamma_2^R} \right), \quad (16)$$

then

$$\frac{\gamma_1^R}{\gamma_1^L} = \frac{\gamma_2^R}{\gamma_2^L}. \quad (17)$$

Substituting condition (16) into Eq. (13), one can make sure that in terms of the exact eigenvalues ($\varepsilon_{1,2}$), the BIC energy (15) becomes either $E_{\text{BIC}} = \varepsilon_1$ or $E_{\text{BIC}} = \varepsilon_2$ depending on the relative sign of matrix elements Δ , $\gamma_1^{L,R}$ and $\gamma_2^{L,R}$. The condition (16) can be rewritten in this case as

$$\varepsilon_2 - \varepsilon_1 = \pm \Delta \left| \frac{\gamma_2^L}{\gamma_1^L} + \frac{\gamma_1^L}{\gamma_2^L} \right| = \pm \Delta \left| \frac{\gamma_2^R}{\gamma_1^R} + \frac{\gamma_1^R}{\gamma_2^R} \right|, \quad (18)$$

where sign in the right-hand side is chosen appropriately.

Here we have studied the well-known model of Friedrich and Wintgen [4] in the case of two continua, which is typical for quantum transport problems. In general, system coupled to two continua should have three degenerate states to possess a BIC [40,50,51]. However, as we have shown, the specific condition of proportionate coupling (17) establishes the formal equivalence between two and single continua because it reduces the rank of the self-energy matrix to one. The same result can be derived in the standard notion of Feshbach's effective Hamiltonian (see Appendix B). It can be illustratively interpreted as follows. The FW mechanism assumes some proper relation between wave-function amplitudes corresponding to interfering states. At the same time, proportionate coupling condition (17) ensures that the same relation holds for states in both incoming and outgoing channels. It is important to note that condition (17) concerns just two close eigenstates regardless of couplings for all the rest levels. Thus, we explicitly show that the FW mechanism of BIC formation can take place even if the input and output waveguides are not equivalent geometrically and the system does not possess any symmetry. This conclusion represents the key result of our paper.

We admit that a very specific situation can exist if the ratio of C_1 and C_2 (or C_3 and C_4) is real. In this

case resultant (14) turns to zero also for $\varepsilon_2^0 - \varepsilon_1^0 = \Delta(\gamma_2^L/\gamma_1^L - \gamma_1^L/\gamma_2^L) + C_2/C_1(\gamma_1^R/\gamma_1^L - \gamma_2^R/\gamma_2^L)$ or $\varepsilon_2^0 - \varepsilon_1^0 = \Delta(\gamma_2^R/\gamma_1^R - \gamma_1^R/\gamma_2^R) + C_4/C_3(\gamma_2^L/\gamma_2^R - \gamma_1^L/\gamma_1^R)$. Moreover, one must additionally check that the common root of $P(E)$ and $Q(E)$ is real. Satisfying all these conditions simultaneously seems to be highly unlikely in general.

In some cases, e.g., in symmetric systems, energies of the eigenstates of the isolated quantum system can demonstrate crossing with a possibility of degeneracy. Analysis of such systems can be performed via general expressions above with $\Delta = 0$ and $\varepsilon_{1,2}^0 = \varepsilon_{1,2}$. Thus, BIC formation still requires proportionate coupling (17), but condition (16) or (18) is replaced by the requirement of degeneracy: $\varepsilon_1 = \varepsilon_2$.

In general, one can distinguish three qualitatively different configurations fulfilling the proportionate coupling condition (17):

$$\gamma_1^L = \gamma_1^R \quad \text{and} \quad \gamma_2^L = \gamma_2^R, \quad (19a)$$

$$\gamma_1^L = -\gamma_1^R \quad \text{and} \quad \gamma_2^L = -\gamma_2^R, \quad (19b)$$

$$\gamma_1^R/\gamma_1^L = \gamma_2^R/\gamma_2^L \quad \text{for} \quad |\gamma_1^L| \neq |\gamma_1^R| \quad \text{and} \quad |\gamma_2^L| \neq |\gamma_2^R|. \quad (19c)$$

The case (19a) takes place if, for example, the system with waveguides is mirror-symmetric and states |1) and |2) are of the same parity; whereas the case (19b) corresponds, for instance, to the configuration invariant under central point reflection (centrosymmetric) with states |1) and |2) being of the opposite parity. Such BICs were studied in various structures [8–10]. On the other hand, BIC in the case (19c) arises in a system coupled to waveguides in some arbitrary asymmetric way, which, to our concern, was not discussed in the literature before. In the next sections, we provide examples of such BICs in asymmetric configurations of quantum billiards and optical waveguides.

It should be noted that BIC energy (15) and conditions (16) and (17) are derived under the assumption of a single (propagating) transverse mode in each electrode. However, typically attached waveguides or electrodes provide many transverse modes. In the energy range, where there is only one propagating mode, the rest are evanescent but they do influence the interference in the quantum transport. This influence arises due to nonzero Hermitian parts of the evanescent modes self-energies. One can take it into account following the general multiterminal approach [41] (see Appendix C for details). Thus, in general, Eqs. (15)–(17) provide only a good initial guess for finding an exact position of BIC.

C. Transmission coefficient near BIC

It is known that the transmission coefficient is discontinuous at the very point of BIC formation in the energy-parameters space [5–8,14,22]. Thus, analysis of the

transmission spectrum behavior near BIC deserves special attention. In order to perform such analysis, we introduce some detuning parameters a and b , which describe the deviation from the conditions (16) and (17) respectively:

$$\begin{aligned} a &= \varepsilon_2^0 - \varepsilon_1^0 - \Delta \left(\frac{\gamma_2^L}{\gamma_1^L} - \frac{\gamma_1^L}{\gamma_2^L} \right), \\ b &= \frac{\gamma_1^R}{\gamma_1^L} - \frac{\gamma_2^R}{\gamma_2^L}. \end{aligned} \quad (20)$$

Expansion of functions P and Q near $E = E_{\text{BIC}}$ in terms of variables a and b gives

$$P(E) \approx C_P \times (E - E_P), \quad Q(E) \approx C_Q \times (E - E_Q), \quad (21)$$

where $C_{P,Q}$ are some scaling prefactors and

$$\begin{aligned} E_P &= E_{\text{BIC}} + R_a a + R_{aa}^P a^2 + R_{ab}^P ab, \\ E_Q &= E_{\text{BIC}} + R_a a + R_{aa}^Q a^2 + R_{ab}^Q ab + R_{bb}^Q b^2 \\ &\quad + i(I_{aa}^Q a^2 + I_{ab}^Q ab + I_{bb}^Q b^2) \end{aligned} \quad (22)$$

are the roots of the P and Q functions respectively. Here real coefficients R_a , R_{aa}^P , R_{ab}^P , R_{bb}^P , I_{aa}^Q , I_{ab}^Q , and I_{bb}^Q are some cumbersome functions of microscopic parameters of the system. For a qualitative analysis one can treat them as some phenomenological values.

Figure 2 depicts the typical behavior of the transmission coefficient evolution near BIC. The graphs are plotted according to Eqs. (21) and (22) with the following phenomenological parameters (in arbitrary units) $R_a = 1$, $R_{aa}^P = 2$, $R_{ab}^P = -0.5$, $R_{aa}^Q = -0.9$, $R_{ab}^Q = 1.3$, $R_{bb}^Q = 2$, $I_{aa}^Q = 0.1$, $I_{ab}^Q = -0.4$, and $I_{bb}^Q = 0.2$. Situation with $b = 0$, shown in Fig. 2(c), corresponds to the exact fulfillment of condition (17) taking place either in mirror-symmetric systems or in systems invariant under central point reflection. In the next section such behavior of the transmission coefficient is confirmed in 2D quantum billiards and optical resonators.

III. NUMERICAL SIMULATIONS

A. Quantum billiard

Consider a 2D rectangle resonator attached to two electronic waveguides (Fig. 3). One can deal with the scattering problem for this system by solving a 2D Schrödinger equation

$$\frac{\partial^2 \Psi(x, y)}{\partial x^2} + \frac{\partial^2 \Psi(x, y)}{\partial y^2} + [E - U(x, y)]\Psi(x, y) = 0 \quad (23)$$

with appropriate boundary conditions on $\Psi(x, y)$. For definiteness we assume that the potential energy $U(x, y)$ vanishes in the internal region and is kept constant and equal to $U_0 = 1$ eV in the external region of the billiard. Effective mass of electron is set to $m = 0.0665m_0$.

The geometry of the considered system provides the following potential profile

$$U(x, y) = \begin{cases} U_L(y), & x \leq 0, \\ U_0(y), & 0 < x \leq L, \\ U_R(y), & x > L, \end{cases} \quad (24)$$

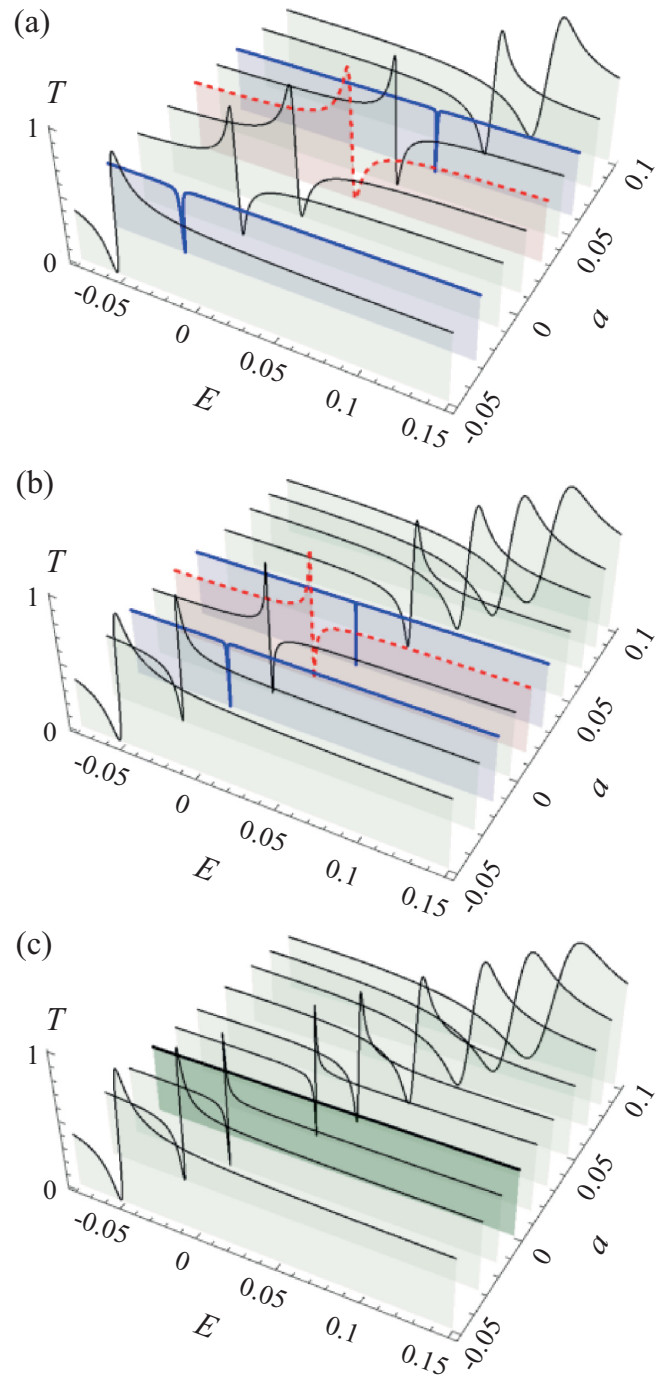


FIG. 2. Typical evolution of the transmission coefficient in the vicinity of BIC with varying detuning a for $b = 0.05$ (a), $b = 0.025$ (b), and $b = 0$ (c). Blue solid thick lines highlight transmission spectra with symmetric Fano antiresonance, and red dashed thick lines correspond to spectra with unity peak. BIC takes place for $a = b = 0$ and corresponds to smooth transmission shown by the thick black line in part (c).

where $U_{L,R}(y)$ defines the transverse potential in the left or right waveguide, and $U_0(y)$ is the transverse potential in the resonator region of length L . Schrödinger equation (23) with $U(x, y)$ from Eq. (24) allows variable separation, and the general solution in each region (left waveguide, resonator, right

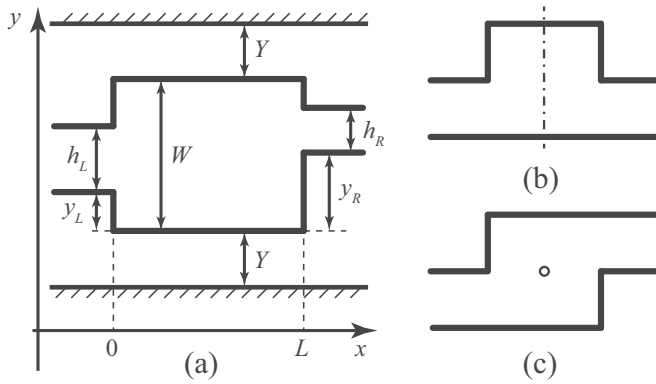


FIG. 3. General schematic view of the 2D quantum billiard attached to two electronic waveguides (a). Mirror-symmetric system with $h_L = h_R$ and $y_L = y_R$ (b) and configuration invariant under central point reflection with $h_L = h_R$ and $y_L = W - h_{L,R} - y_R$ (c).

waveguide) can be written as [52–55]

$$\Psi_j(x, y) = \sum_n (A_n^j e^{ik_n^j x} + B_n^j e^{-ik_n^j x}) \Phi_n^j(y). \quad (25)$$

Here $k_n^j = 1/\hbar\sqrt{2m(E - \alpha_n^j)}$ is the wave number along the propagation direction, j labels one of the regions in (24) and n stands for the transverse quantization mode number. Transverse wave functions $\Phi_n^j(y)$ with corresponding eigenvalues α_n^j are found from the effective 1D Schrödinger equation:

$$\frac{d^2 \Phi_n^j(y)}{dy^2} + [\alpha_n^j - U_j(y)] \Phi_n^j(y) = 0. \quad (26)$$

We consider the energy range, where there is only a single propagating mode in each waveguide: $E \in (\max(\alpha_1^L, \alpha_1^R), \min(\alpha_2^L, \alpha_2^R))$. For the particular values of the left and right waveguides width ($h_L = 5$ nm and $h_R = 4$ nm), the energy range we focus on becomes $E \in (183, 506)$ meV.

Summation in Eq. (25) is performed over all infinite number of transverse modes in the j th region, including both states of discrete and continuous spectra. The latter is simulated by a dense set of discrete states formed between artificial borders with infinite potential along the x axis at some distance Y from the resonator. Continuous spectrum corresponds to the limit $Y \rightarrow \infty$. However, a finite value of Y can be defined from the convergence conditions of the results. Within this section, we perform calculations for $W = 10$ nm, in which case $Y = 10$ nm is enough. The convergence condition also defines the total number of transverse modes taken into account, and for our calculation, it is typically about 30–40.

According to Eq. (16) initial guess on the BIC conditions and energy can be based on analysis of the spectrum of the localized states of the isolated structure (without waveguides). Localized states of a rectangle quantum billiard can be found in factorized form:

$$\psi_{(n_x, n_y)}(x, y) = \chi_{n_x}(x) \phi_{n_y}(y), \quad (27)$$

where quantum numbers $n_x - 1$ and $n_y - 1$ define the number of nodes of $\psi_{(n_x, n_y)}(x, y)$ in x and y directions, respectively. Figure 4 shows energy of such localized states (n_x, n_y) with varying length of the resonator. BICs are expected near the

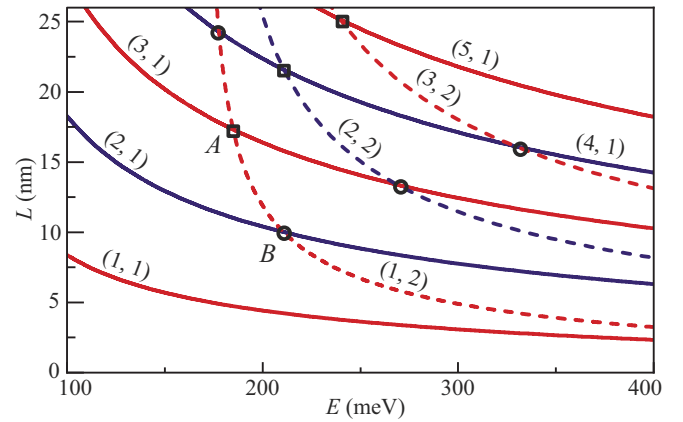


FIG. 4. Energies of localized states $\psi_{(n_x, n_y)}$ of a closed 2D billiard with $W = 10$ nm and different values of L . Red lines indicate symmetric states, and blue lines antisymmetric. BICs are labeled by black open squares for mirror-symmetric system and by black open circles for centrosymmetric system. Due to evanescent modes in the waveguides, BICs do not coincide perfectly with points of degeneracy, even in symmetric configurations.

points of degeneracy. To be specific we focus on those labeled as A and B in Fig. 4 with $E_A \approx 184.98$ meV, $L_A \approx 17.3314$ nm and $E_B \approx 210.82$ meV, $L_B = 10$ nm.

Configurations with mirror symmetry [Fig. 3(b)] and invariant under central point reflection, i.e., centrosymmetric [Fig. 3(c)], are known to possess BICs [8,9], and hence it is illustrative to begin our discussion from these cases. As was discussed above, condition (19a) implies that BICs in mirror-symmetric structures arise for the states of the same parity [$n_{x,1} \equiv n_{x,2} \pmod{2}$], shown by open black squares in Fig. 4, and condition (19b) provides BICs in centrosymmetric systems from the states of the opposite parity [$n_{x,1} - n_{x,2} \equiv 1 \pmod{2}$], represented by open black circles in Fig. 4.

Parameters of the attached waveguides and the incident electron energy are chosen to provide just a single propagating mode in each waveguide (all the other modes are evanescent). Thus, couplings of localized states in the resonator with the continuum in left or right waveguide are equal to the couplings with the single propagating mode [8,56]:

$$\gamma_{(n_x, n_y)}^{L,R} = \left. \frac{\partial \chi_{n_x}(x)}{\partial x} \right|_{x=0,L} \mu_{1n_y}^{L,R}. \quad (28)$$

Here

$$\mu_{1n_y}^{L,R} = \int \phi_1^{L,R}(y) \phi_{n_y}(y) dy \quad (29)$$

is the corresponding element of the unitary matrix connecting transverse modes in the waveguide and the resonator. In particular, $\phi_1^{L,R}(y)$ is the y -component of the first transverse mode in the left or right waveguide.

In the present paper we focus on the possibility for BIC formation in asymmetric systems, and hence we study quantum billiard with waveguides of different sizes ($h_L \neq h_R$). In this case condition (17) in its most general form (19c) is not fulfilled automatically, as in the discussed above symmetric cases. Therefore, some parameters should be additionally

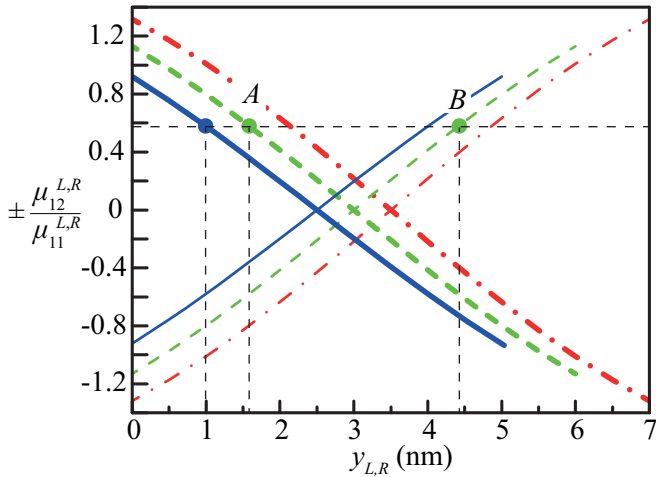


FIG. 5. Positive (thick lines) and negative (thin lines) ratio $\mu_{12}^{L,R}/\mu_{11}^{L,R}$ vs. position of the waveguide $y_{L,R}$ for $h_{L,R} = 5$ nm (solid blue lines), $h_{L,R} = 4$ nm (dashed green lines), and $h_{L,R} = 3$ nm (dot-dashed red lines).

tuned to satisfy it. In case of the considered rectangle resonator, condition (19c) applied for two states $(n_{x,1}, n_{y,1})$ and $(n_{x,2}, n_{y,2})$ with couplings (28) reduces to

$$\frac{\mu_{1n_{y,1}}^L}{\mu_{1n_{y,2}}^L} = \pm \frac{\mu_{1n_{y,1}}^R}{\mu_{1n_{y,2}}^R}. \quad (30)$$

Plus sign in Eq. (30) corresponds to the case $n_{x,1} \equiv n_{x,2} \pmod{2}$, and minus sign $-$ to $n_{x,1} - n_{x,2} \equiv 1 \pmod{2}$. We consider only the first two transverse modes in the resonator, and hence $n_{y,1}$ and $n_{y,2}$ can be either 1 or 2. According to Fig. 4, the states with the same n_y cannot become degenerate. Thus, we analyze condition (30) only for $n_{y,1} = 1$ and $n_{y,2} = 2$ or vice versa.

Ratios μ_{12}^L/μ_{11}^L and μ_{12}^R/μ_{11}^R in Eq. (30) depend similarly on h_L, y_L or h_R, y_R respectively. Figure 5 depicts the ratio $\mu_{12}^{L,R}/\mu_{11}^{L,R}$ as a function of $y_{L,R}$ for different values of $h_{L,R}$. This diagram allows one, for instance, to determine parameters of the right waveguide (h_R and y_R), which satisfy condition (30), for a given parameters of the left waveguide (h_L and y_L). For $h_L = 5$ nm and $y_L = 1$ nm it provides $\mu_{12}^L/\mu_{11}^L \approx 0.57494$ (blue dot in Fig. 5). The same ratio for the right waveguide with $h_R = 4$ nm takes place for either $y_R^A = 1.5871$ nm (green point A in Fig. 5) if we take sign plus in Eq. (30), or $y_R^B = 4.4129$ nm (green point B in Fig. 5) if we take minus plus in Eq. (30). The former case corresponds to the nearly mirror-symmetric configuration and the latter $-$ to the nearly centrosymmetric one. Thus, the initial guess for the BIC conditions and energy can be made from Fig. 4 for L and E and from Fig. 5 for h_R and y_R . Taking other transverse modes into account results in a slight violation of the exact BIC parameters from these estimations, as is shown below.

We determine the exact position of BIC from a precise numerical solution of the scattering problem. In general, localized states of the billiard manifest themselves as Fano resonances [57] in the transmission spectrum. The width of this resonance ΔE , i.e., energy split between the peak and the

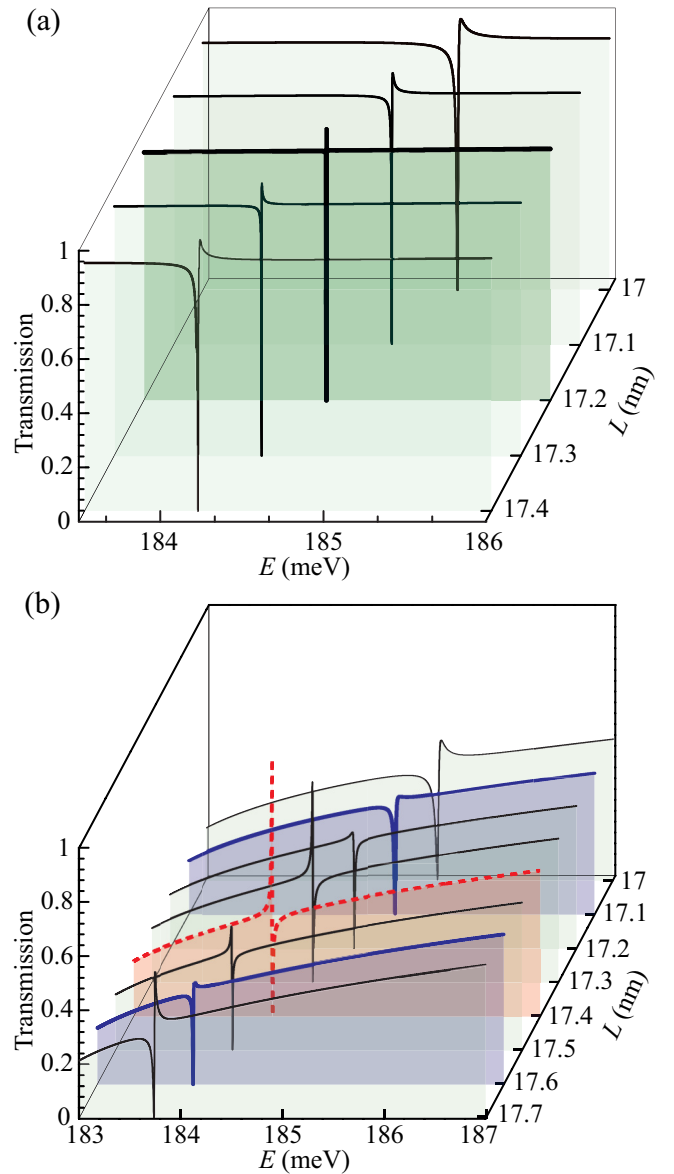


FIG. 6. Evolution of the transmission spectrum of the mirror-symmetric system with $h_R = h_L = 5$ nm and $y_R = y_L = 1$ nm for different values of L (a). Evolution of the transmission spectrum of an asymmetric system with $h_R = 4$ nm and $y_R = 1.45$ nm for different values of L (b). In part (b), blue solid thick lines highlight transmission spectra with symmetric Fano antiresonance, and red dashed thick lines correspond to spectra with unity peak.

dip, shrinks when approaching the BIC point, where it turns to zero exactly [14,22].

For a mirror-symmetric [Fig. 3(b)] or centrosymmetric system [Fig. 3(c)] with $h_L = h_R$, condition (30) and hence condition (17) are fulfilled automatically due to the symmetry. Thus, for such systems, ΔE varies monotonically with L and it turns to zero from some L_{BIC} , which is close to either L_A or L_B depending on the considered structure. Figure 6(a) shows $T(E)$ vs. L evolution for the mirror-symmetric configuration with $h_R = h_L = 5$ nm and $y_R = y_L = 1$ nm. In this case L_{BIC} is about $L_{\text{BIC}} \approx 17.2180$ nm that is pretty close to the initial estimation L_A (Fig. 4). One can admit that qualitative behavior

of the transmission spectrum shown in Fig. 6 agrees well with the phenomenological model in Fig. 2(c).

In the case of an asymmetric system, the behavior of the transmission coefficient with varying L becomes more complicated. Figure 6(b) depicts the evolution of $T(E)$ with varying L for a system with $h_R = 4$ nm and $y_R = 1.45$ nm, which is close to the condition of exact proportionality of the couplings (point A in Fig. 5). Similar $T(E)$ behavior is observed for a wide range of y_R values. By analogy with symmetric configurations, there is a range of L values, where ΔE decreases. However, here it changes slightly and remains finite within this range. Transmission peak value T_{\max} also behaves in a complicated manner. First, it decreases with decreasing width, and at some L , the $T(E)$ curve turns into a symmetric Fano antiresonance – it does not have a maximum at all within the range of interest [blue graph in Fig. 6(b)]. Then T_{\max} increases and reaches unity without any considerable change of the resonance width [red dashed graph in Fig. 6(b)]. Further tuning of L again provides the situation with the absence of a maximum, after which a significant increase in the resonance width begins. When approaching the BIC, along with a decrease in the widths of resonances, the distance in energy between symmetric Fano antiresonances (Fano resonances without peak) also decreases and vanishes at the BIC point exactly. The observed behavior of the transmission spectrum fully agrees with the phenomenological model proposed in Figs. 2(a) and 2(b).

Exactly at the BIC energy and corresponding parameters, the transmission peak and the dip must coincide [14]. Thus, we apply the following algorithm to find exact BIC conditions and energy. For each value of y_R , we find L , which provides a transmission spectrum with a unity peak. Energy difference ΔE between this resonance and zero-valued dip in the transmission is treated as a Fano resonance width associated with given y_R and L . Figure 7(a) illustrates the dependence $\Delta E(y_R)$. The BIC corresponds to the point $\Delta E = 0$. It is important to show that ΔE does vanish at some point instead of having a local minimum, where it remains small but finite. The inset shows the region near the minimum with a much smaller scale. Precise parameter tuning allows one to make ΔE close to zero with any accuracy. Thus, we prove that there is the true BIC for a system with completely asymmetric waveguides attachment.

In L - E plane positions of the transmission peaks and the dips are shown in Fig. 7(b). They coincide at the BIC which is slightly shifted from the degeneracy point A due to the multiple evanescent modes taken into account in numerical calculations. In this case the BIC occurs at $E_{\text{BIC},A} \approx 184.64213$ meV for $y_R^{\text{BIC},A} \approx 1.5574$ nm and $L_{\text{BIC},A} \approx 17.2696$ nm. These parameters are pretty close to the initial estimations derived from the general conditions (16) and (17), i.e., from the requirement of degeneracy (point A in Fig. 4) and proportionate coupling (point A in Fig. 5). In the same way, BIC for another pair of degenerate states (point B in Fig. 4) can be analyzed. The transmission peaks and the dips are shown in Fig. 7(c), and BIC takes place for $y_R^{\text{BIC},B} \approx 4.4419$ nm and $L_{\text{BIC},B} \approx 9.9703$ nm at energy $E_{\text{BIC},B} \approx 209.61988$ meV that is again close to the initial guess. All these results are summarized in Table I.

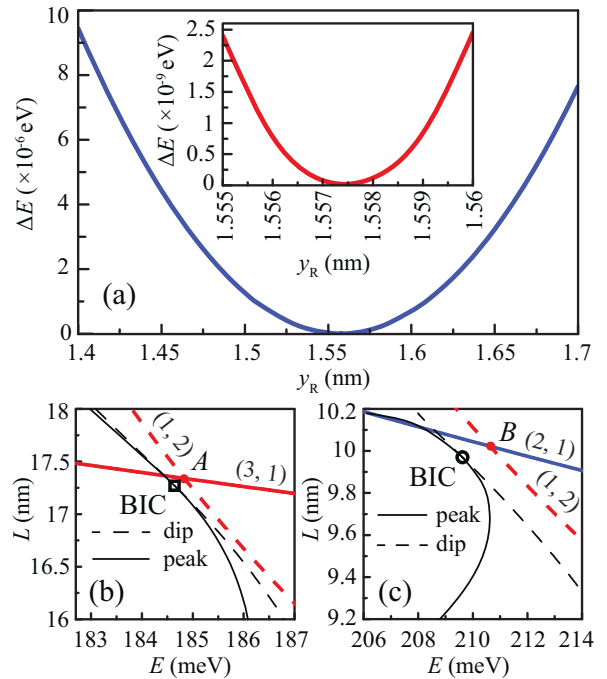


FIG. 7. Minimal Fano resonance width ΔE vs. position of the right waveguide y_R for $h_R = 4$ nm, $h_L = 5$ nm, $W = 10$ nm, and $y_L = 1$ nm (a). Energies of the localized state (3,1) and (1,2) of the closed billiard (red thick solid line and red thick dashed line respectively) near the degeneracy point A (see Fig. 4) in the L - E plane (b). Energies of the localized states (2,1) and (1,2) (blue thick solid line and red thick dashed line respectively) near the degeneracy point B (see Fig. 4) in the L - E plane (c). BICs are located where transmission peak (black thin solid lines) meets transmission dip (black thin dashed lines).

It is illustrative to trace the probability density distribution in the structure corresponding to a BIC. Figure 8 shows the probability distributions for situations A and B. The interference contribution of states (1,2) and (3,1) is clearly manifested in BIC corresponding to the case A [Fig. 8(a)], and states (1,2) and (2,1) of isolated billiards appear in the case B [Fig. 8(b)]. The calculations also show that the scattering wave function at the energies of maximum and minimum transmission near the BIC is close to the corresponding BIC wave function, as it should be according to the general theory [14].

TABLE I. BICs energy and parameters in 2D quantum billiard.

	Initial guess from conditions (16) and (17)	Exact values
Nearly mirror-symmetric	$E_A \approx 184.98$ meV $L_A \approx 17.3314$ nm $y_R^A \approx 1.5871$ nm	$E_{\text{BIC},A} \approx 184.64213$ meV $L_{\text{BIC},A} \approx 17.2696$ nm $y_R^{\text{BIC},A} \approx 1.5574$ nm
Nearly centro-symmetric	$E_B \approx 210.82$ meV $L_B = 10$ nm $y_R^B \approx 4.4129$ nm	$E_{\text{BIC},B} \approx 209.61988$ meV $L_{\text{BIC},B} \approx 9.9703$ nm $y_R^{\text{BIC},B} \approx 4.4419$ nm

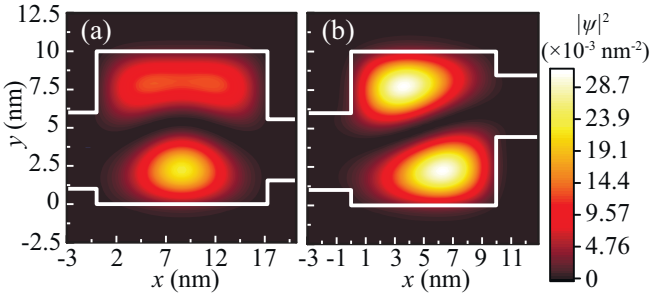


FIG. 8. Probability density distribution of BIC states in the quantum billiard. Parameters are the following: $W = 10$ nm, $y_L = 1$ nm, $h_L = 5$ nm, $h_R = 4$ nm, and (a) $y_R = y_R^{\text{BIC},A} \approx 1.5574$ nm, $L = L_{\text{BIC},A} \approx 17.2696$ nm, $E = E_{\text{BIC},A} \approx 184.64213$ meV or (b) $y_R = y_R^{\text{BIC},B} \approx 4.4419$ nm, $L = L_{\text{BIC},B} \approx 9.9703$ nm, $E = E_{\text{BIC},B} \approx 209.61988$ meV.

B. Cavity in optical waveguide

Due to the natural correspondence between 2D Schrödinger and scalar Helmholtz equations [58], one can expect effects of BIC formation in an optical waveguide with a cavity. We consider a 2D dielectric optical structure with geometry similar to Fig. 3(a). In optics, we use wavelength λ instead of energy (or frequency). Two-dimensional Helmholtz equation for TE wave can be written as follows [58]:

$$\frac{\partial^2 E(x, y)}{\partial x^2} + \frac{\partial^2 E(x, y)}{\partial y^2} + \left[\frac{2\pi}{\lambda} n(x, y) \right]^2 E(x, y) = 0, \quad (31)$$

where $E(x, y)$ is the electric field and λ is the radiation wavelength. The refractive index distribution $n(x, y)$ in the considered system can be described by the step-like function along the propagation coordinate similar to the potential energy of a 2D quantum billiard (24), [Fig. 3(a)]:

$$n(x, y) = \begin{cases} n_L(y), & x \leq 0, \\ n_0(y), & 0 < x < L, \\ n_R(y), & x > L, \end{cases} \quad (32)$$

The waveguides and the resonator (cavity) in (32), shown in Fig. 3(a), have refractive index $n = 1.5$, while the refractive index of environment is $n_0 = 1$. With Eq. (32) taken into account, the Helmholtz equation (31) can be solved by variable separation similar the Schrödinger equation (23). Its general solution takes the form (25) with $k_n^j = 2\pi/\lambda\sqrt{\beta_n^j}$, where β_n^j is derived from the following effective 1D equation:

$$\frac{d^2 \Phi_n^j(y)}{dy^2} + \left(\frac{2\pi}{\lambda} \right)^2 [n_f^j(y) - \beta_n^j] \Phi_n^j(y) = 0. \quad (33)$$

BIC is a zero-width state of an open system. The lifetime of a BIC may be considered infinite. In general, finite width transforms a BIC into a decaying state, which manifests itself in scattering as a Fano resonance [6,7,14,22]. In quantum mechanics, bound states of an electronic billiard, which are responsible for Fano resonances in the scattering of propagating mode in the waveguide, correspond to the decaying modes. Such modes have energies below the levels of transverse quantization in the waveguide ($E < \alpha$).

Contrary to quantum mechanics, in purely dielectric waveguides, we have no cutoff frequencies (energies), and de-

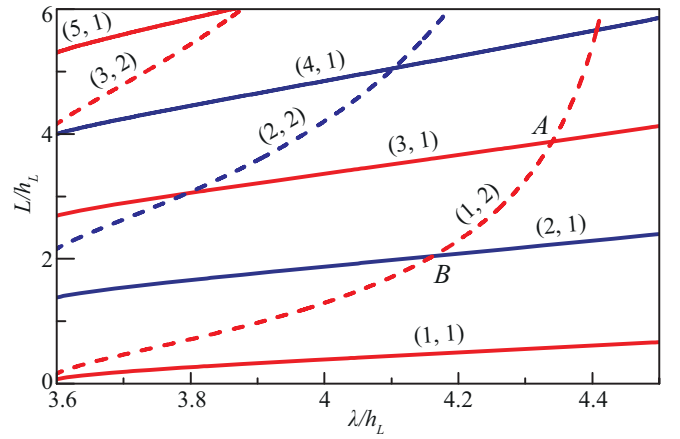


FIG. 9. Wavelengths of localized modes in the cavity with $W = 10$ nm and different values of L . Red lines indicate symmetric states and blue lines antisymmetric.

caying modes in the propagation direction (in our case $-x$) do not exist. To have true bound states with $\beta < 0$ in the propagation direction, one should either confine electromagnetic field in the transverse direction as in metal waveguide [58] (analogue of size quantization) or use an “extra dimension” [59] (propagating wave has a component in direction orthogonal to the 2D system [60], z in our case). These conditions produce an effect of the evanescent waves in the waveguide propagation direction. Here we imply the first option and insert our dielectric waveguide between two ideally conducting metal plates, located at some distance Y from the cavity (Fig. 3). The electric field of the TE-wave takes zero values at these plates. Thus, in this case, the numerical result depends strongly on Y . However, the qualitative conclusions on the BIC formation are universal, as shown above in the theoretical section, and hence we focus on the simplest situation with $Y = 0$. Here again we focus on the wavelength range, where there is only a single propagating mode in each waveguide, i.e., $\beta_1^{L,R} > 0$ and $\beta_n^{L,R} < 0$ for $n = 2, 3, 4, \dots$. For the particular geometry we consider ($h_R = 0.8h_L$), the wavelength range becomes $3.588h_L < \lambda < 6.459h_L$.

In order to study BIC formation in a way similar to the quantum billiard, we start with the determination of geometric parameters of the resonator providing degenerate eigenmodes. Without loss of generality, we normalize all lengths in the considered problem to the width of the left waveguide h_L . Figure 9 depicts the wavelengths of some cavity modes depending on its length L for $W = 3h_L$. According to the condition (16), BICs are expected in the vicinity of degeneracies, i.e., intersection points. We focus on two degeneracies – labeled as A and B in Fig. 9, where $\lambda_A \approx 4.34079h_L$, $L_A \approx 3.87591h_L$ and $\lambda_B \approx 4.16243h_L$, $L_B \approx 3.03912h_L$. Like in the case of quantum billiard, point A corresponds to a field distribution symmetric along the x axis, and point B to a centrosymmetric configuration. Positions of the waveguides $y_{L,R}$ do not significantly change cavity eigenmodes. Therefore, it can serve as a reference point for the search for a BIC in systems with asymmetric attached waveguides.

In quantum mechanics, energy enters the Schrödinger equation linearly, whereas, in optics, the Helmholtz equation

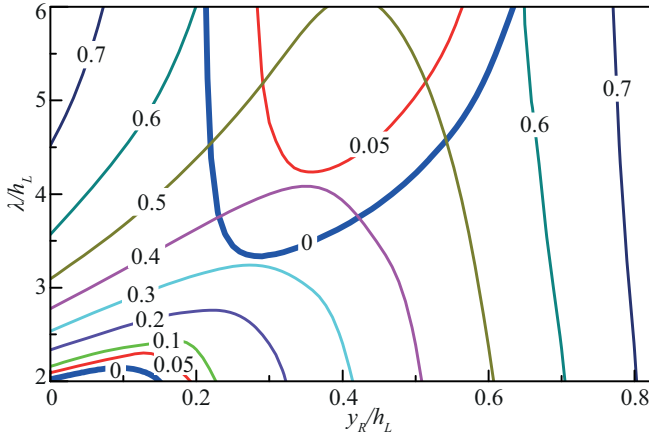


FIG. 10. Set of graphical solutions for the proportionate coupling condition (30) with plus sign (for nearly mirror-symmetric system). Number near each line indicates corresponding y_L value in units of h_L . The rest parameters are as follows $W = 3h_L$, $h_R = 0.8h_L$, and $Y = 0$.

is quadratic in wavelength. It leads to wavelength dependency of the effective refractive index, making the computation more sophisticated. To determine the parameters of the asymmetric system, we set the width of the left waveguide y_L , and for each y_L we find the values of y_R and the wavelength λ , which ensure the fulfillment of condition (30), i.e., condition (17). As a result, one can obtain a family of curves $\lambda(y_R)$ for different values of y_L . Figure 10 depicts these curves for the plus sign in condition (30), i.e., for the nearly mirror-symmetric configurations with $y_R < \frac{1}{2}(W - h_R)$. A similar diagram can be obtained for the nearly centrosymmetric configuration as well. As one can see from Fig. 10, in contrast to quantum billiards, there is the possibility for a BIC at two values of y_R for the nearly mirror-symmetric configuration and at two values of y_R for nearly centrosymmetric configuration. In particular, one gets $y_R^{A,1} \approx 0.2205h_L$, $y_R^{A,2} \approx 0.5152h_L$ for $\lambda = \lambda_A$, and $y_R^{B,1} \approx 1.708h_L$, $y_R^{B,2} \approx 1.9773h_L$ for $\lambda = \lambda_B$.

Typical transmission spectrum $T(\lambda)$ of an optical system near a BIC behaves similarly to the quantum billiard and corresponds to the phenomenological model shown in Figs. 2(a) and 2(b). There is a region of L values, which provides a small width of the Fano resonance, with a curve reaching $T_{\max} = 1$ and symmetric Fano antiresonances with no peaks nearby. BICs can be found in the same way as in the case of quantum billiard. For each y_R we find L , which provides $T_{\max} = 1$, and evaluate the corresponding Fano resonance width $\Delta\lambda$. Then, we make sure that minimum $\Delta\lambda(y_R)$ vanishes at some critical value of y_R , which implies a BIC formation.

Figure 11(a) shows the $\Delta\lambda(y_R)$ dependence near point A in Fig. 9 (nearly mirror-symmetric case). Two zero minima are observed: the first at $y_R^{\text{BIC},A,1} \approx 0.2229h_L$, corresponding to $\lambda_{\text{BIC},A,1} \approx 4.33878h_L$, $L_{\text{BIC},A,1} \approx 3.8619h_L$, and the second at $y_R^{\text{BIC},A,2} \approx 0.4864h_L$, with $\lambda_{\text{BIC},A,2} \approx 4.33826h_L$, $L_{\text{BIC},A,2} \approx 3.8746h_L$. It should be noted that between these minimal values, $\Delta\lambda$ remains quite small, i.e., the system can possess a resonator with a high Q factor in a wide range of parameters. The intensity distribution in this case is qualitatively similar to the BIC in the quantum billiard [Fig. 8(a)].

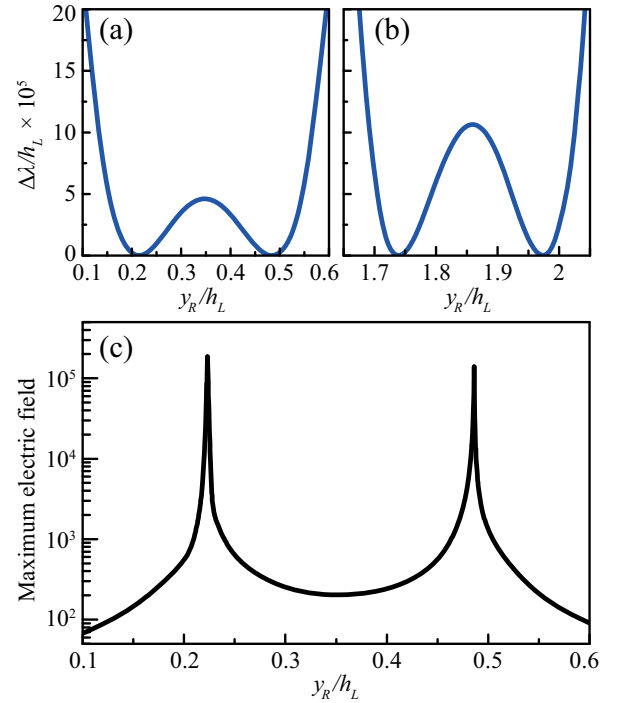


FIG. 11. Minimal Fano resonance width $\Delta\lambda$ vs. position of the right waveguide y_R for nearly mirror-symmetric (a) and nearly centrosymmetric (b) configuration. Dependence of the maximum value of the electric field in the cavity on y_R for wavelengths corresponding to $T = 0$. Parameters are $y_L = 0$, $h_R = 0.8h_L$, and $W = 3h_L$.

A similar dependence of the Fano resonance width is obtained for the nearly centrosymmetric case [Fig. 11(b)]. BIC formation again takes place at two points: the first at $y_R^{\text{BIC},B,1} \approx 1.7394h_L$, $L_{\text{BIC},B,1} \approx 2.0329h_L$, and $\lambda_{\text{BIC},B,1} \approx 4.15393h_L$ and the second at $y_R^{\text{BIC},B,2} \approx 1.9742h_L$, $L_{\text{BIC},B,2} \approx 2.0209h_L$, and $\lambda_{\text{BIC},B,2} \approx 4.15539h_L$. The intensity distribution in this case is qualitatively the same as the the BIC density distribution in quantum billiard [Fig. 8(b)]. All the results for an optical waveguide with a cavity are summarized in Table II.

TABLE II. BICs wavelength and parameters in 2D optical waveguide with cavity.

	Initial guess from conditions (16) and (17)	Exact values
Nearly mirror-symmetric	$\lambda_A \approx 4.34079h_L$	$\lambda_{\text{BIC},A,1} \approx 4.33878h_L$
	$L_A \approx 3.87591h_L$	$L_{\text{BIC},A,1} \approx 3.8619h_L$
	$y_R^{A,1} \approx 0.2205h_L$	$y_R^{\text{BIC},A,1} \approx 0.2229h_L$
	$y_R^{A,2} \approx 0.5152h_L$	$y_R^{\text{BIC},A,2} \approx 0.4864h_L$
Nearly centrosymmetric	$\lambda_B \approx 4.16243h_L$	$\lambda_{\text{BIC},B,1} \approx 4.15393h_L$
	$L_B \approx 3.03912h_L$	$L_{\text{BIC},B,1} \approx 2.0329h_L$
	$y_R^{B,1} \approx 1.708h_L$	$y_R^{\text{BIC},B,1} \approx 1.7394h_L$
	$y_R^{B,2} \approx 1.9773h_L$	$y_R^{\text{BIC},B,2} \approx 1.9742h_L$

An additional criterion for BIC formation can be the divergence of the intensity in the cavity when approaching BIC in this wavelength-parameters space. Figure 11(c) shows the dependence for the maximum electric field modulus $|E_{\max}|$ in the structure and is normalized by electric field amplitude of the incident wave in the first mode of the left waveguide. Sharp increase in $|E_{\max}|$ is observed near the points of $\Delta\lambda$ vanishing.

IV. CONCLUSION

Design of structures with embedded BICs is of primary importance not only for fundamental study of interference phenomena but for a large number of applications based on high- Q resonances such as Refs. [1,2,21]. BICs in past years have been studied in a tremendous number of electronic and electromagnetic structures, the vast majority of which are symmetric. BIC energies and corresponding system's parameters can be determined by finding a root of some single variable functions in spatially symmetric structures. In the general case of asymmetric structures, the problem becomes multiparametric and much more cumbersome.

It was shown by Pavlov-Verevkin and coauthors in Ref. [40] that, in general, an N -level system coupled to K continua can support $N - K$ BICs if all N states are degenerate. However, if the rank of the coupling matrix becomes lower than K (due to the collinearity of the coupling vectors), then the number of BICs can be increased. Our paper extends this idea to consider not only degenerate states forming BIC and to include all the rest eigenstates. At the same time, our approach generalizes the FW model and is applicable to the avoided crossing case as well. We have shown explicitly how the condition of proportionate coupling (collinearity of the coupling vectors) arises in the case of two continua that are represented by two geometrically different waveguides. Therefore, in the limiting case of the level crossing, where degeneracy is possible, our condition requires the degeneracy of only two levels instead of three according to the general statement of Pavlov-Verevkin as discussed in, e.g., Refs. [50,51].

In this paper, we have developed principal design rules (16) and (17) for constructing spatially nonsymmetric electronic and electromagnetic systems with BICs originated from the FW mechanism. Our approach is based on the analysis of

BIC formation via a unified theory of transport phenomena in quantum conductors, which can be applied with equal success to both tight-binding and continuous models. The analytic results are formulated in terms of energy levels of the isolated system and couplings with the input and output waveguides. The particular meaning of such couplings is different in tight-binding and continuous approaches, but, as our numerical simulations show, the formulated rule works well in both limits. Physically, the ratio of wave function (light field) amplitudes providing destructive interference in the coupling of the quantum state (resonator's mode) with the continuum should be the same for both waveguides, i.e., the condition of proportionate coupling should be fulfilled. In fact, it means that though the system possesses two geometrically different input and output waveguides, it can be considered within a single channel scattering problem. Analytic derivation of the proportionate coupling condition is performed by considering a single propagating mode in each waveguide. Hence this condition is not exact. However, as our results show, it can serve as an excellent initial guess for the search of BIC location points using multimode numerical modeling.

In practice, BICs are typically revealed as extremely high- Q resonances. Such resonances find many applications, mainly in optics, including enhancement of light-matter interaction for lasing and harmonic generation, efficient light guiding, and sensing [21]. We believe that the proposed idea of proportionate coupling and the results of our paper broadens the class of structures allowing for the BIC formation, which can benefit in a wide range of wave phenomena.

ACKNOWLEDGMENT

We acknowledge the Russian Science Foundation for support under Project No. 21-19-00808.

APPENDIX A: $P(E)$ AND $Q(E)$ FUNCTIONS NEAR BIC

In the vicinity of BIC, where exact eigenvalues $\varepsilon_{1,2}$ are close to each other, we use the two-level reparametrization (12) and get the following approximation for functions from Eq. (11):

$$\begin{aligned}
 F_{LL}(E) &\approx \frac{(E - \varepsilon_1^0)(\gamma_2^L)^2 + (E - \varepsilon_2^0)(\gamma_1^L)^2 + 2\Delta\gamma_1^L\gamma_2^L}{(E - \varepsilon_1^0)(E - \varepsilon_2^0) - \Delta^2} + C_{LL}, \\
 F_{RR}(E) &\approx \frac{(E - \varepsilon_1^0)(\gamma_2^R)^2 + (E - \varepsilon_2^0)(\gamma_1^R)^2 + 2\Delta\gamma_1^R\gamma_2^R}{(E - \varepsilon_1^0)(E - \varepsilon_2^0) - \Delta^2} + C_{RR}, \\
 F_{LR}(E) &\approx \frac{(E - \varepsilon_1^0)\gamma_2^L\gamma_2^R + (E - \varepsilon_2^0)\gamma_1^L\gamma_1^R + \Delta(\gamma_1^L\gamma_2^R + \gamma_1^R\gamma_2^L)}{(E - \varepsilon_1^0)(E - \varepsilon_2^0) - \Delta^2} + C_{LR}.
 \end{aligned} \tag{A1}$$

Here C_{LL} , C_{RR} , and C_{LR} take into account the contribution from all the rest energy levels ($i \neq 1, 2$), which we take as constants in the energy range of interest. Hereinafter, we restrict $\gamma_{1,2}^{L,R}$ and C_{LR} to be real quantities, all the rest parameters

are real by their definition. Substituting Eqs. (A1) into Eqs. (9) and (10), one can get approximated expressions for $P(E)$ and $Q(E)$ functions near BIC. One should be cautious that exactly at BIC [under conditions (16) and (17)] numerator and

denominator of functions (A1) turn to zero simultaneously at $E = E_{\text{BIC}}$.

APPENDIX B: BIC FROM THE EFFECTIVE HAMILTONIAN PERSPECTIVE

The exact expression for the effective Hamiltonian (7) of the N -level two-terminal quantum conductor is derived by the Feshbach's projection operator technique [46]. Analysis of its properties in the vicinity of ε_1 and ε_2 can be performed in the same manner—by projection onto the subspace of states $|1\rangle$ and $|2\rangle$. Thus, effective Hamiltonian of these two states incorporating waveguides self-energies and influence of all the rest states of the quantum conductor can be written in the following form:

$$\hat{H}_{2 \times 2}^{\text{eff}} = \hat{H}_{2 \times 2} + \hat{\Sigma}. \quad (\text{B1})$$

Here $\hat{H}_{2 \times 2}$ is defined in Eq. (12) and $\hat{\Sigma}$ is the total self-energy:

$$\hat{\Sigma} = \hat{\Sigma}_L + \hat{\Sigma}_R - \hat{\Sigma}_{LR}, \quad (\text{B2})$$

with

$$\hat{\Sigma}_{L,R} = \tilde{\mathbf{u}}_{L,R} \tilde{\mathbf{u}}_{L,R}^\dagger \left[2 - \frac{1 - C_{RR,LL} \sigma_{R,L}}{D} \right] \sigma_{L,R}, \quad (\text{B3})$$

$$\hat{\Sigma}_{LR} = (\tilde{\mathbf{u}}_L \tilde{\mathbf{u}}_R^\dagger + \tilde{\mathbf{u}}_R \tilde{\mathbf{u}}_L^\dagger) \sigma_L \sigma_R \frac{C_{LR}}{D}, \quad (\text{B4})$$

where $\sigma_{L,R} = h_{L,R} - i g_{L,R}$, $\tilde{\mathbf{u}}_{L,R} = (\gamma_1^{L,R}, \gamma_2^{L,R})^\top$, and

$$D = [1 - C_{LL} \sigma_L] \times [1 - C_{RR} \sigma_R] - C_{LR} \sigma_L \sigma_R. \quad (\text{B5})$$

Couplings $\gamma_{1,2}^{L,R}$ are energy-independent and quantities C_{LL} , C_{RR} , C_{LR} , $h_{L,R}$, and $g_{L,R}$ are defined in Sec. II B.

Condition of proportionate coupling (17) results in $\tilde{\mathbf{u}}_L \propto \tilde{\mathbf{u}}_R$, which in turn implies $\hat{\Sigma}_L \propto \hat{\Sigma}_R \propto \hat{\Sigma}_{LR}$ according to Eqs. (B3) and (B4). Therefore, under this condition non-Hermitian part of the effective Hamiltonian (B1) has rank 1. Hence $\hat{H}_{2 \times 2}^{\text{eff}}$ can have a real eigenvalue, i.e., BIC formation takes place, due to the Friedrich-Wintgen mechanism if the condition (16) is fulfilled.

APPENDIX C: TAKING EVANESCENT MODES IN WAVEGUIDES INTO ACCOUNT

Coupling of the N -level quantum system to $K_{L,R} + 1$ channels in the left or right electrode (waveguide) respectively can be described by introduction of the corresponding self-energies. Hermitian and anti-Hermitian parts of this self-energies are given similarly to Eqs. (4) but with $N \times (K_{L,R} + 1)$ coupling matrices $\hat{G}_{L,R}(E)$ [and their Hilbert transforms $\hat{H}_{L,R}(E)$] instead of $N \times 1$ coupling matrices (vectors) $\mathbf{u}_{L,R}$ defined in Eq. (5) [43]:

$$\begin{aligned} \hat{\Gamma}_{L,R}(E) &= \hat{G}_{L,R}(E) \hat{G}_{L,R}^\dagger(E), \\ \hat{\delta}_{L,R}(E) &= \hat{H}_{L,R}(E) \hat{H}_{L,R}^\dagger(E). \end{aligned} \quad (\text{C1})$$

We assume that there is a single propagating channel in each electrode and $K_{L,R}$ evanescent modes, respectively. Due to the orthogonality of different modes, one can treat each channel as an independent terminal. Thus, Eq. (C1) may be

rewritten similarly to the multiterminal case [41]:

$$\begin{aligned} \hat{\Gamma}_{L,R}(E) &= \mathbf{u}_{L,R} \mathbf{u}_{L,R}^\dagger g_{L,R}(E), \\ \hat{\delta}_{L,R}(E) &= \mathbf{u}_{L,R} \mathbf{u}_{L,R}^\dagger h_{L,R}(E) + \sum_{i=1}^{K_{L,R}} \mathbf{u}_{L,R;i} \mathbf{u}_{L,R;i}^\dagger h_{L,R;i}(E). \end{aligned} \quad (\text{C2})$$

Here $\mathbf{u}_{L,R}$, $g_{L,R}(E)$, and $h_{L,R}(E)$ are introduced in Sec. II B. Quantities $\mathbf{u}_{L,R;i}$ and $h_{L,R;i}(E)$ are defined similarly, but correspond to the i th mode in the left or right electrode. Substituting Eqs. (C2) into (6), one can derive the transmission coefficient in the same form (8) with $P(E)$ and $Q(E)$ functions given by Eqs. (9) and (10) but with hybridized Hamiltonian

$$\hat{H}_{\text{hyb}} = \hat{H}_0 + \sum_{i=1}^{K_L} \mathbf{u}_{L,i} \mathbf{u}_{L,i}^\dagger h_{L,i}(E) + \sum_{i=1}^{K_R} \mathbf{u}_{R,i} \mathbf{u}_{R,i}^\dagger h_{R,i}(E) \quad (\text{C3})$$

instead of the bare Hamiltonian of the isolated system \hat{H}_0 . Thus, states $|1\rangle$ and $|2\rangle$ should be considered as eigenstates of the hybridized Hamiltonian (C3).

Nevertheless, one can rewrite $P(E)$ and $Q(E)$ functions in terms of the eigenstates of the isolated system. In this case all Eqs. (8)–(10) remain the same but with F_{LL} , F_{RR} , and F_{LR} replaced by

$$\begin{aligned} \mathcal{F}_{ab} &= F_{ab} + (\mathbf{F}_{aL}^\dagger \quad \mathbf{F}_{aR}^\dagger) \left[\begin{pmatrix} \hat{1}_{K_L} & 0 \\ 0 & \hat{1}_{K_R} \end{pmatrix} - \begin{pmatrix} \hat{f}_{LL} & \hat{f}_{LR} \\ \hat{f}_{RL} & \hat{f}_{RR} \end{pmatrix} \right]^{-1} \\ &\quad \times \begin{pmatrix} \mathbf{F}_{bL} \\ \mathbf{F}_{bR} \end{pmatrix}. \end{aligned} \quad (\text{C4})$$

Here subscripts a, b show the correspondence either to the left or right waveguide (i.e., $a, b \in \{L, R\}$), functions F_{ab} are from Eq. (11), and $\hat{1}_{K_{L,R}}$ is the identity matrix of dimension $K_{L,R}$. Components of the K_L -dimensional vectors \mathbf{F}_{LL} and \mathbf{F}_{RL} and K_R -dimensional column-vectors \mathbf{F}_{LR} and \mathbf{F}_{RR} are defined as follows:

$$[\mathbf{F}_{ab}]_i = \sqrt{h_{b;i}(E)} \sum_{k=1}^N \frac{\gamma_k^a \gamma_k^{b;i*}}{E - \varepsilon_k}, \quad (\text{C5})$$

where $\gamma_k^{L,R;i}$ is the k th element of the coupling vector $\mathbf{u}_{L,R;i}$. Similarly, one can write matrix elements of \hat{f}_{LL} , \hat{f}_{LR} , \hat{f}_{RL} , and \hat{f}_{RR} :

$$[\hat{f}_{ab}]_{ij} = \sqrt{h_{a;i}(E) h_{b;j}(E)} \sum_{k=1}^N \frac{\gamma_k^{a;i*} \gamma_k^{b;j}}{E - \varepsilon_k}. \quad (\text{C6})$$

The absolute strength of the evanescent modes influence is governed by the functions $h_{L,R;i}(E)$, whereas the relative strength of the evanescent modes influence on different eigenstates of the isolated system is defined through $\gamma_k^{L,R;i}$. In general, derivation of an exact condition for BIC formation in terms of isolated quantum system eigenstates is extremely tough. However, if the influence of the evanescent modes is weak, then one can assume that functions \mathcal{F}_{ab} from Eqs. (C4) differ only slightly from those without evanescent modes taken into account: F_{ab} given by Eq. (11). Therefore, in general, we expect the BIC formation not exactly for the conditions (15)–(17), but in some vicinity of them in the energy-parameters space.

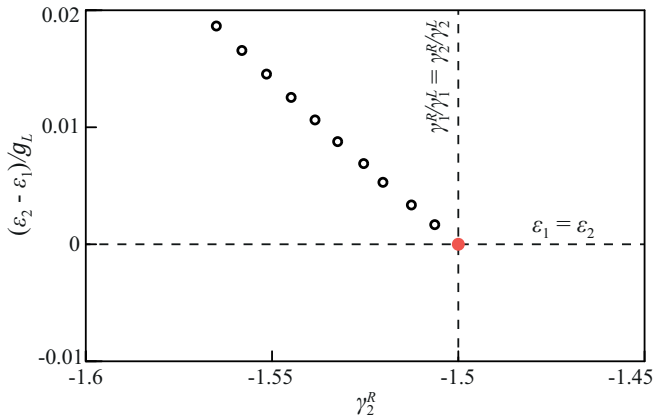


FIG. 12. Parameters corresponding to BIC formation for different strength of the evanescent modes influence. Red solid circle shows the parameters of BIC formation without evanescent modes taken into account. Black open circles correspond to BIC with $h_{R,1} = 0.5h_{L,1}$ and $h_{L,1}$ varying from 0 to $-0.1g_L$ with a $-0.01g_L$ step.

As an example, we consider the simplest case with one evanescent mode in each waveguide ($K_L = K_R = 1$). In this situation, vectors (C5) and matrices (C6) will be just 1×1 scalars. In the vicinity of two eigenstates with close energies ε_1 and ε_2 , one can approximate Eqs. (C5) and (C6) similar to

Eq. (A1). For simplicity we consider the case, when crossing of ε_1 and ε_2 is possible ($\Delta = 0$), and get:

$$\begin{aligned} [\mathbf{F}_{ab}]_i &\approx \sqrt{h_{b,1}} \left(\frac{\gamma_1^a \gamma_1^{b,1}}{E - \varepsilon_1} + \frac{\gamma_2^a \gamma_2^{b,1}}{E - \varepsilon_2} + A_{ab} \right), \\ [\hat{f}_{ab}]_1 &\approx \sqrt{h_{a,1} h_{b,1}} \left[\frac{\gamma_1^{a,1} \gamma_1^{b,1}}{E - \varepsilon_1} + \frac{\gamma_2^{a,1} \gamma_2^{b,1}}{E - \varepsilon_2} + B_{ab} \right]. \end{aligned} \quad (\text{C7})$$

Here constants A_{ab} and B_{ab} take into account eigenstates beyond $|1\rangle$ and $|2\rangle$. We also assume that all tunneling couplings are real and we approximate functions $h_{L,R;1}(E)$ as energy-independent constants $h_{L,R;1}$ in the energy range of interest.

In Fig. 12, we show the positions of BIC in the parameter space of $\Delta\varepsilon = \varepsilon_2 - \varepsilon_1$ and γ_2^R for different influence strength of the evanescent modes (different values of $h_{L,R;1}$). Parameters are set as follows: $\gamma_1^L = 0.3$, $\gamma_1^R = -0.5$, $\gamma_2^L = 0.9$, $C_{LL} = 0.1g_L^{-1}$, $C_{RR} = 0.02g_L^{-1}$, $C_{LR} = -0.08g_L^{-1}$, $g_R = 0.5g_L$, $h_L = 0.4g_L$, $h_R = -0.1g_L$, $A_{LL} = 0.1g_L^{-1}$, $A_{RR} = -0.18g_L^{-1}$, $A_{LR} = 0.14g_L^{-1}$, $A_{RL} = 0.02g_L^{-1}$, $B_{LL} = 0.06g_L^{-1}$, $B_{RR} = 0.12g_L^{-1}$, $B_{LR} = -0.08g_L^{-1}$, $\gamma_1^{L;1} = 0.9$, $\gamma_1^{R;1} = 0.5$, $\gamma_2^{L;1} = -0.5$, and $\gamma_2^{R;1} = 0.4$. Without evanescent modes taken into account BIC formation takes place exactly for conditions (16) and (17), which are shown by dashed lines in Fig. 12.

-
- [1] C. W. Hsu, B. Zhen, A. D. Stone, J. D. Joannopoulos, and M. Soljačić, Bound states in the continuum, *Nat. Rev. Mater.* **1**, 16048 (2016).
- [2] A. F. Sadreev, Interference traps waves in open system: Bound states in the continuum, *Rep. Prog. Phys.* **84**, 055901 (2021).
- [3] J. von Neuman and E. Wigner, Über merkwürdige diskrete Eigenwerte, *Phys. Z.* **30**, 465 (1929).
- [4] H. Friedrich and D. Wintgen, Interfering resonances and bound states in the continuum, *Phys. Rev. A* **32**, 3231 (1985).
- [5] C. S. Kim, A. M. Satanin, Y. S. Joe, and R. M. Cosby, Resonant tunneling in a quantum waveguide: Effect of a finite-size attractive impurity, *Phys. Rev. B* **60**, 10962 (1999).
- [6] M. L. LadroneGuevara, F. Claro, and P. A. Orellana, Ghost fano resonance in a double quantum dot molecule attached to leads, *Phys. Rev. B* **67**, 195335 (2003).
- [7] M. L. Ladrón de Guevara and P. A. Orellana, Electronic transport through a parallel-coupled triple quantum dot molecule: Fano resonances and bound states in the continuum, *Phys. Rev. B* **73**, 205303 (2006).
- [8] A. F. Sadreev, E. N. Bulgakov, and I. Rotter, Bound states in the continuum in open quantum billiards with a variable shape, *Phys. Rev. B* **73**, 235342 (2006).
- [9] A. Lyapina, A. Pilipchuk, and A. Sadreev, Bound states with orbital angular momentum in the continuum of cylindrical non-axisymmetric waveguide, *Ann. Phys.* **396**, 56 (2018).
- [10] T. Lepetit and B. Kanté, Controlling multipolar radiation with symmetries for electromagnetic bound states in the continuum, *Phys. Rev. B* **90**, 241103(R) (2014).
- [11] A. I. Ovcharenko, C. Blanchard, J.-P. Hugonin, and C. Sauvan, Bound states in the continuum in symmetric and asymmetric photonic crystal slabs, *Phys. Rev. B* **101**, 155303 (2020).
- [12] K. Koshelev, S. Lepeshov, M. Liu, A. Bogdanov, and Y. Kivshar, Asymmetric Metasurfaces with High- q Resonances Governed by Bound States in the Continuum, *Phys. Rev. Lett.* **121**, 193903 (2018).
- [13] G. Ordóñez, K. Na, and S. Kim, Bound states in the continuum in quantum-dot pairs, *Phys. Rev. A* **73**, 022113 (2006).
- [14] A. A. Gorbatshevich and N. M. Shubin, Unified theory of resonances and bound states in the continuum in hermitian tight-binding models, *Phys. Rev. B* **96**, 205441 (2017).
- [15] C. S. Kim and A. M. Satanin, Dynamic confinement of electrons in time-dependent quantum structures, *Phys. Rev. B* **58**, 15389 (1998).
- [16] G. Della Valle and S. Longhi, Floquet-hubbard bound states in the continuum, *Phys. Rev. B* **89**, 115118 (2014).
- [17] A. F. Sadreev and T. V. Babushkina, Two-electron bound states in a continuum in quantum dots, *JETP Lett.* **88**, 312 (2008).
- [18] M. A. Sierra, M. Saiz-Bretín, F. Domínguez-Adame, and D. Sánchez, Interactions and thermoelectric effects in a parallel-coupled double quantum dot, *Phys. Rev. B* **93**, 235452 (2016).
- [19] S. V. Aksenov and M. Y. Kagan, Collapse of the fano resonance caused by the nonlocality of the majorana state, *JETP Lett.* **111**, 286 (2020).
- [20] N. Shubin, A. Emelianov, Y. Uspenskii, and A. Gorbatshevich, Interacting resonances and antiresonances in conjugated hydrocarbons: Exceptional points and bound states in the continuum, *Phys. Chem. Chem. Phys.* (2021), doi:10.1039/D1CP02504J.

- [21] S. I. Azzam and A. V. Kildishev, Photonic bound states in the continuum: From basics to applications, *Adv. Opt. Mater.* **9**, 2001469 (2021).
- [22] C. Blanchard, J.-P. Hugonin, and C. Sauvan, Fano resonances in photonic crystal slabs near optical bound states in the continuum, *Phys. Rev. B* **94**, 155303 (2016).
- [23] A. Kodigala, T. Lepetit, Q. Gu, B. Bahari, Y. Fainman, and B. Kanté, Lasing action from photonic bound states in continuum, *Nature (Lond.)* **541**, 196 (2017).
- [24] S. Mizuno, Fano resonances and bound states in the continuum in a simple phononic system, *Appl. Phys. Express* **12**, 035504 (2019).
- [25] Z. Yu, X. Xi, J. Ma, H. K. Tsang, C.-L. Zou, and X. Sun, Photonic integrated circuits with bound states in the continuum, *Optica* **6**, 1342 (2019).
- [26] E. A. Bezus, D. A. Bykov, and L. L. Doskolovich, Bound states in the continuum and high-q resonances supported by a dielectric ridge on a slab waveguide, *Photon. Res.* **6**, 1084 (2018).
- [27] F. Yesilkoy, E. R. Arvelo, Y. Jahani, M. Liu, A. Tittl, V. Cevher, Y. Kivshar, and H. Altug, Ultrasensitive hyperspectral imaging and biodetection enabled by dielectric metasurfaces, *Nat. Photon.* **13**, 390 (2019).
- [28] P. S. Pankin, B.-R. Wu, J.-H. Yang, K.-P. Chen, I. V. Timofeev, and A. F. Sadreev, One-dimensional photonic bound states in the continuum, *Commun. Phys.* **3**, 91 (2020).
- [29] A. S. Kupriyanov, Y. Xu, A. Sayanskiy, V. Dmitriev, Y. S. Kivshar, and V. R. Tuz, Metasurface Engineering Through Bound States in The Continuum, *Phys. Rev. Appl.* **12**, 014024 (2019).
- [30] D. R. Abujetas, N. van Hoof, S. ter Huurne, J. G. Rivas, and J. A. Sánchez-Gil, Spectral and temporal evidence of robust photonic bound states in the continuum on terahertz metasurfaces, *Optica* **6**, 996 (2019).
- [31] Y. Plotnik, O. Peleg, F. Dreisow, M. Heinrich, S. Nolte, A. Szameit, and M. Segev, Experimental Observation of Optical Bound States in the Continuum, *Phys. Rev. Lett.* **107**, 183901 (2011).
- [32] K.-K. Voo and C. S. Chu, Localized states in continuum in low-dimensional systems, *Phys. Rev. B* **74**, 155306 (2006).
- [33] S. Weimann, Y. Xu, R. Keil, A. E. Miroschnichenko, A. Tünnermann, S. Nolte, A. A. Sukhorukov, A. Szameit, and Y. S. Kivshar, Compact Surface Fano States Embedded in the Continuum of Waveguide Arrays, *Phys. Rev. Lett.* **111**, 240403 (2013).
- [34] B. Deb and G. S. Agarwal, Creation and manipulation of bound states in the continuum with lasers: Applications to cold atoms and molecules, *Phys. Rev. A* **90**, 063417 (2014).
- [35] V. A. Sablikov and A. A. Sukhanov, Helical bound states in the continuum of the edge states in two dimensional topological insulators, *Phys. Lett. A* **379**, 1775 (2015).
- [36] Y. Boretz, G. Ordonez, S. Tanaka, and T. Petrosky, Optically tunable bound states in the continuum, *Phys. Rev. A* **90**, 023853 (2014).
- [37] T. Lepetit, E. Akmansoy, J.-P. Ganne, and J.-M. Lourtioz, Resonance continuum coupling in high-permittivity dielectric metamaterials, *Phys. Rev. B* **82**, 195307 (2010).
- [38] A. Lyapina, A. Pilipchuk, and A. Sadreev, Trapped modes in a non-axisymmetric cylindrical waveguide, *J. Sound Vib.* **421**, 48 (2018).
- [39] S. Mukherjee, J. Gomis-Bresco, P. Pujol-Closa, D. Artigas, and L. Torner, Topological properties of bound states in the continuum in geometries with broken anisotropy symmetry, *Phys. Rev. A* **98**, 063826 (2018).
- [40] F. Remacle, M. Munster, V. Pavlov-Verevkin, and M. Desouter-Lecomte, Trapping in competitive decay of degenerate states, *Phys. Lett. A* **145**, 265 (1990).
- [41] N. M. Shubin, A. A. Gorbatsevich, and G. Y. Krasnikov, Non-hermitian hamiltonians and quantum transport in multi-terminal conductors, *Entropy* **22**, 459 (2020).
- [42] V. Sokolov and V. Zelevinsky, Collective dynamics of unstable quantum states, *Ann. Phys.* **216**, 323 (1992).
- [43] A. Volya and V. Zelevinsky, Non-hermitian effective hamiltonian and continuum shell model, *Phys. Rev. C* **67**, 054322 (2003).
- [44] J. C. Cuevas and E. Scheer, *Molecular Electronics: An Introduction to Theory and Experiment* (World Scientific, Singapore, 2010).
- [45] S. Datta, *Electronic Transport in Mesoscopic Systems*, Cambridge Studies in Semiconductor Physics (Cambridge University Press, Cambridge, 1997).
- [46] H. Feshbach, Unified theory of nuclear reactions, *Ann. Phys.* **5**, 357 (1958).
- [47] J. Sherman and W. J. Morrison, Adjustment of an inverse matrix corresponding to a change in one element of a given matrix, *Ann. Math. Stat.* **21**, 124 (1950).
- [48] D. A. Harville, *Matrix Algebra from a Statistician's Perspective*, Vol. 1 (Springer, New York, 1997).
- [49] A. Pilipchuk and A. Sadreev, Accidental bound states in the continuum in an open sinai billiard, *Phys. Lett. A* **381**, 720 (2017).
- [50] E. Bulgakov and A. Sadreev, Formation of bound states in the continuum for a quantum dot with variable width, *Phys. Rev. B* **83**, 235321 (2011).
- [51] A. S. Pilipchuk, A. A. Pilipchuk, and A. F. Sadreev, Multi-channel bound states in the continuum in coaxial cylindrical waveguide, *Phys. Scr.* **94**, 115004 (2019).
- [52] G. N. Henderson, T. K. Gaylord, and E. N. Glytsis, Ballistic electron transport in semiconductor heterostructures and its analogies in electromagnetic propagation in general dielectrics, *Proc. IEEE* **79**, 1643 (1991).
- [53] M. Asada, Y. Miyamoto, and Y. Suematsu, Gain and the threshold of three-dimensional quantum-box lasers, *IEEE J. Quant. Electron.* **22**, 1915 (1986).
- [54] J. Sánchez-Dehesa, J. A. Porto, F. AgullóRueda, and F. Meseguer, Electronic energy levels of quantum-well wires, *J. Appl. Phys.* **73**, 5027 (1993).
- [55] A. A. Gorbatsevich and V. V. Kapaev, Waveguide nanoelectronics, *Russ. Microelectr.* **36**, 1 (2007).
- [56] K. Pichugin, H. Schanz, and P. Seba, Effective coupling for open billiards, *Phys. Rev. E* **64**, 056227 (2001).
- [57] U. Fano, Effects of configuration interaction on intensities and phase shifts, *Phys. Rev.* **124**, 1866 (1961).
- [58] J. D. Joannopoulos, S. G. Johnson, J. N. Winn, and R. D. Meade, *Photonic Crystals* (Princeton University Press, Princeton, NJ, 2011).
- [59] D. Dragoman and M. Dragoman, Optical analogue structures to mesoscopic devices, *Prog. Quant. Electron.* **23**, 131 (1999).
- [60] D. Dragoman and M. Dragoman, Optical modeling of quantum wire arrays, *IEEE J. Quant. Electron.* **33**, 375 (1997).